Evaluation of the Dose Distribution Gradient in the Close Vicinity of Brachytherapy Seeds Using Electron Paramagnetic Resonance Imaging

Emilia S. Vanea,[1] Philippe Levêque,[1] Fadi Abboud,[2] Anne Bol,[2] Jean Marc Denis,[2] Natallia Kolbun,[1] Stefaan Vynckier,[2] and Bernard Gallez[1]*

Electron paramagnetic resonance (EPR) spectroscopy has been successfully employed to determine radiation dose using alanine. The EPR signal intensity reflects the number of stable free radicals produced, and provides a quantitative measurement of the absorbed dose. The aim of the present study was to explore whether this principle can be extended to provide information on spatial dose distribution using EPR imaging (EPRI). Lithium formate was selected because irradiation induces a single EPR line, a characteristic that is particularly convenient for imaging purposes. ^{125}I-brachytherapy seeds were inserted in tablets made of lithium formate. Images were acquired at 1.1 GHz. Monte Carlo (MC) calculations were used for comparison. The dose gradient can be determined using two-dimensional (2D) EPR images. Quantitative data correlated with the dose estimated by the MC simulations, although differences were observed. This study provides a first proof-of-concept that EPRI can be used to estimate the gradient dose distribution in phantoms after irradiation. Magn Reson Med 61:1225–1231, 2009. © 2009 Wiley-Liss, Inc.

Key words: EPR; free radicals; dosimetry; dose distribution; brachytherapy

Low dose rate (LDR) brachytherapy via permanently implanted Iodine-125 or Palladium-103 seeds (~30 keV photons with a dose-reduction factor of about 10 for 1 cm of tissue) is frequently used to treat tumors, prostate cancer in particular, but also eye tumors. The advantages of low energy are that radioprotection for medical workers is easier and there is a confined volume of radiation dose from the implant. When performing a clinical treatment, it is mandatory to very precisely report various parameters that can impact patient treatment outcome. These parameters include the prescribed dose, the doses received by various organs, and the degree of dose uniformity that will be achieved on the target and in the surrounding healthy tissues. It is clear that to achieve good precision in the treatment itself, the source dosimetry must be established with a maximum of accuracy. As dosimetric characteristics at these low energies are very dependent on the internal design of the implant, any new source design must undergo detailed evaluation (1). Generally, dosimetric characteristics are determined using Monte Carlo (MC) simulations. However, such calculations can give different results depending on the MC calculation codes used. These can differ in their basic data or in the approximations made in the underlying physics (2). Experimentally, dosimetry could be performed using thermoluminescent (TLD) dosimeters. However, to obtain data with a high spatial resolution is still challenging because of the large gradient of dose and the very LDR. In this context, there is still a need to develop experimental methods that allow estimation of the dose deposited in the proximity of brachytherapy seeds. The present study attempted to develop a new method based on the reconstruction of dose using electron paramagnetic resonance (EPR) imaging (EPRI).

EPR dosimetry (3) is the determination of dose by measuring radiation-induced free radicals in irradiated materials using EPR. The EPR signal intensity directly reflects the number of stable free radicals produced in a solid matrix, providing a quantitative measurement of the absorbed dose. The major advantages of an EPR dosimeter are its small physical size and that no cables or auxiliary equipment are required during the measurements. Further, the nondestructive readout allows repeated calibration and accumulated doses to be measured. Alanine is the best known dosimeter material, already suggested for this purpose more than 40 years ago and now formally accepted by the International Atomic Energy Agency (IAEA) as a standard for high-dose (0.1–100 kGy) and transfer dosimetry. The alanine response varies little with radiation energy, dose rate, temperature, and time between irradiation and readout. In brachytherapy, alanine pellets have been used to determine the dose at discrete points around ^{192}Ir and ^{137}Cs sources (4−6).

Formates (salts of formic acid, HCOOH) were suggested as alternatives to alanine a few years ago (7,8). Lithium formate shows great potential for accurately determining low radiation doses (9). Lithium formate is about six times more sensitive than alanine, shows a linear dose response up to 1 kGy, and is close to water in terms of absorption properties and scattering of radiation. It also has a high resistance to fading if it is kept in correct conditions (low humidity and dark) after irradiation. Moreover, the EPR

spectrum of irradiated polycrystalline lithium formate consists of a single EPR line. This latter characteristic is particularly useful for imaging purpose with EPRI.

Using appropriate field gradients, EPRI can map the distribution of free radicals inside samples in two or three dimensions. This method is analogous to MRI, except that the generated image represents the distribution of electron spins instead of nuclear spins. EPRI has been used in vivo to investigate the distribution of stable free radicals, or to indirectly map important physiological parameters, such as oxygen (10), nitric oxide (11), or redox status (12). In the field of dosimetry, EPRI has been used to retrospectively reconstruct the dose after bone irradiation (13). To our knowledge, the present study is the first attempt to use EPRI as a tool to experimentally evaluate the spatial dose distribution and to apply proof-of-concept to the reconstruction of the gradient of doses surrounding brachytherapy seeds. For this purpose, we developed large cylindrical tablets of lithium formate, in which holes were drilled to allow the insertion of brachytherapy ^{125}I seeds. EPR images of pellets were obtained after irradiation by one or two seeds. Experimental data were compared to MC simulations using MCNP version 4 code (MCNP-4C) (14,15). MC simulation is a statistical solution for complex mathematical problems that uses random sampling. MC simulation of particle transport has become an essential tool for dose calculation in complex medical physics situations, as these calculations are a faithful simulation of physical reality, particularly in situations where measurements are difficult or impossible (16). MCNP, which stands for MC N-Particles, and its precursors, were developed at Los Alamos National Laboratory (Los Alamos, NM, USA) to analyze problems related to nuclear reactors. MCNP-4C is a general-purpose radiation transport code that can be used for coupled neutron/photon/electron transport (17). The code can handle any arbitrary three-dimensional (3D) configuration.

The spatial resolution of EPR images was assessed with a semiempiric method from the edge spread function (ESF).

MATERIALS AND METHODS

Phantoms

Cylindrical tablets (diameter = 22 mm, height = 10 mm) of polycrystalline lithium formate monohydrate (Aldrich, Steinheim, Germany) were made using a tablet press (type AC27, 50 kg/cm²; Ateliers Courtoy, Halle, Belgium). Lithium formate forms strong pellets without need of additional binding material. For brachytherapy studies using one seed, one hole (1.5-mm in diameter) was drilled in the center of the tablet to introduce the radioactive source. For studies with two brachytherapy seeds, two holes (8 mm between centers) were drilled in the tablets.

Irradiation

Some tablets were externally irradiated using an X-ray beam (Philips 250 RT, 250 kV) with a dose rate of 0.85 Gy/min. The samples were irradiated at different doses (25, 50, 100, 200, and 300 Gy) to study the linearity of response. Some of these samples were partially protected

with several layers of lead (triangular shape) to visualize the different nonirradiated shapes. For brachytherapy studies, Iodine-125 seeds (Oncoseed model; GE Healthcare) were used. These seeds consist of a welded titanium capsule (diameter = 0.8 mm, length = 4.5 mm) containing iodine-125 adsorbed onto a silver rod (diameter = 0.5 mm, length = 3 mm). The tablets were irradiated for 2 weeks at room temperature, protected from light and humidity, and kept in the same conditions before being imaged.

EPR Imaging

Since we were interested in radial dosimetry in the phantom, 2D images were acquired along the source perpendicular axis. This allows to build radial dosimetry curves as is commonly performed in similar studies using other methodologies such as film dosimetry. No other 2D orientation nor 3D images were necessary for this work.

The EPR images were acquired at room temperature using an EPR Elexsys E540 System with three orthogonal water-cooled cylindrical gradient coils. The irradiated pellets were placed in the center of an L-Band EPR cylindrical resonator (ER 6502 BC, 23-mm in diameter) operating at 1.1 GHz. The samples were positioned in the EPR resonator with the symmetry axis along the central axis of the cavity. The usual EPRI acquisition parameters were as follows: modulation frequency = 100 kHz, microwave power = 45 mW, modulation amplitude = 3.35 G, 512 points, 30 scans of 5.24 s each, pixel size = 0.5 mm, and spatial window = 30 mm (field of view). The magnitude of the magnetic field gradient was 300 mT/m. 2D images were reconstructed on a 128 × 128 matrix by filtered back-projection using a Shepp-Logan filter (18,19). Before reconstruction, each projection was deconvolved using fast Fourier transform with the measured zero-gradient spectrum to improve image resolution. To reduce noise amplification and avoid possible division by zero at high frequencies, a low-pass filter was used. The deconvolution parameters, including the maximum cutoff frequency and the width of the window in the Fourier space, were set up after viewing the shape of all projections. Data were smoothed using either a Fermi-Dirac or a Gaussian filter.

Spectral deconvolution and filtered backprojection were performed using the Xepr software package (Bruker).

MC Simulations

MCNP-4C was used to calculate the dose distribution around the source. The detailed photon physics option of MCNP was used in this work. This option includes Compton scattering, Rayleigh scattering, and photoelectric effect with emission of fluorescence photons. The cross-section data and the form factors for coherent and incoherent photon scattering were taken from Storm and Israel (14) or from the Evaluated Nuclear Data File (ENDF) (15) while the fluorescence data were taken from Everett and Cashwell (20). A new library of photoelectric cross-sections updated by Bohm et al. (21) was also used. Spheres with a diameter of 0.1 mm defined the acquisition cells (22) at different distances, from −1.1 cm to 1.1 cm. Dose calculations were obtained using the F6 tally card in the MCNP (describing the mean energy deposition per cell in MeV/g),

assuming that electron transport can be neglected at this low photon energy and, consequently, that all electron energy is deposited locally. We modeled the source using data from the literature, and the dosimetric parameters were compared to existing publications to validate our model.

Finally, the number (one billion) of simulation histories was chosen to reduce the maximum statistical uncertainty in the MC calculations to about 2% for a volume element situated at 1.1 cm from the source.

Resolution—ESF Determination

Two different methods were used to assess the resolution of the imaging system.

In the first set of experiments, holes of different diameters (ranging from 5 mm to 2 mm) were drilled in the center of tablets that were subsequently irradiated at 300 Gy with a 6-MeV X-ray beam generated by an Elekta SL75/5 Linac linear accelerator. Image acquisition was performed using the same settings as described in the EPR Imaging section above. The evaluation of the resolution was carried out by visual estimation of images. More formally, the signal falloff in the middle of each image was also measured from the intensity curve using the Xepr software from Bruker.

In the second experiment, the spatial resolution was obtained in terms of the ESF. The ESF was determined following a procedure modified from the classical method used in MRI (23) and from the work of Ahn and Halpern (24–26).

Briefly, a parallelepiped phantom was filled with irradiated (300 Gy) lithium formate. The size of the phantom was 1.0 cm × 1.0 cm × 4.0 cm. A 2D image of the phantom was reconstructed. The signal along a line perpendicular to the edge of the phantom was extracted from the image and the derivative was calculated. A nine-point smoothing algorithm was used to obtain the derivative curve, which was then fitted by a Gaussian function:

$$f(x) = \frac{1}{\sigma \sqrt{2\pi}} e^{-\frac{(x-\mu)^2}{2\sigma^2}}. \qquad [1]$$

From the computed σ values, the full-width at half-maximum (FWHM) of the Gaussian curve was calculated from the following equation:

$$\text{FWHM} = 2.\sigma \sqrt{2.\ln 2}. \qquad [2]$$

All calculations and fitting were carried out using Prism 4 (GraphPad Software, Inc., La Jolla, CA, USA).

RESULTS

The EPR spectrum of irradiated $HCO_2Li \times H_2O$ presented a single-line that was attributed to CO_2^- radicals (Fig. 1a). The EPR signal intensity increased linearly with the dose of external beam irradiation (Fig. 1b), as previously shown (8,9), making this material suitable for dosimetry purposes. Using appropriate field gradients, it was possible to map the distribution of the radiation-induced free radicals
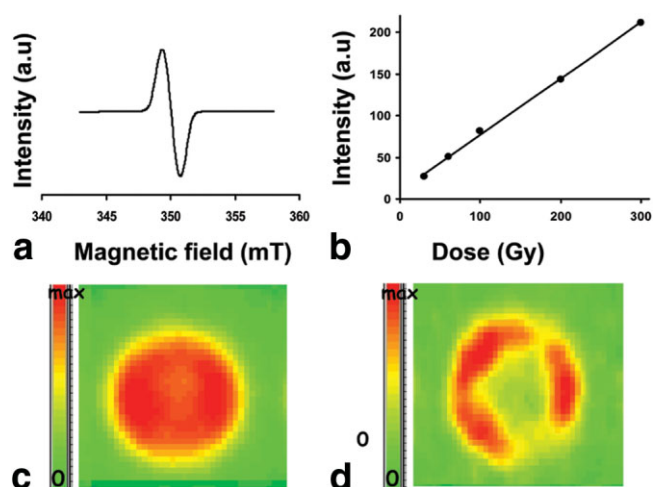
FIG. 1. EPR spectroscopy and imaging on lithium formate samples. **a:** EPR spectrum of externally irradiated lithium formate recorded at 9 GHz. **b:** Dose-response relationship. **c:** EPR image of an externally irradiated tablet of lithium formate. **d:** EPR image of an externally irradiated pellet partly protected by a triangle lead shielding.

in the tablets of lithium formate. The amplitude maps (reflecting the EPR signal intensity) of tablets irradiated by an external source of X-rays are shown in Fig. 1c and d, corresponding to tablets irradiated without lead protection and with a triangular lead protection, respectively. The irradiated zones can be easily visualized in the EPR images, which clearly reflect the known shape and dimensions of the object. The signal is homogenous in each considered zone.

Figure 2a shows the 2D projection of EPR signal intensity surrounding one ^{125}I brachytherapy seed. The shape of the lithium formate tablet is indicated by the black circle. As the EPR signal is proportional to the radiation dose, its variation, depicted by the color code, also reflects the variation of the dose distribution around the seed. Figure 2b is the corresponding wire-frame plot. This is a perspective view of the signal intensity variation inside the phantom. The intensity of the EPR signal reaches its maximum in the middle of the sample, where the seed was inserted, and decreases with distance toward the edges. The radial dose profile, normalized to its maximum, was obtained along the source perpendicular axis and is shown in Fig. 2c. The dose was measured approximately every 1 mm along the axis passing through the center of the tablet.

Figure 3a shows the dose distribution, estimated by the EPR signal intensity, around two ^{125}I radioactive seeds with the same activity, inserted in the phantom lithium formate dosimeter. The distance between two seeds, as measured on the image, is 10 mm. Figure 3b and c present perspective volumes of the doses, and estimated dose distributions (from EPR data) around the seeds.

In Fig. 4, the results of the MC calculations for one seed (Fig. 4a) and two seeds (Fig. 4b) are compared to the experimental data obtained by EPRI. For convenient comparison of EPR and MC curves, data were normalized to the values observed at 1 mm from the center. The first data point of the MC simulation was calculated at 1 mm from the center of the source because: 1) the seed itself was
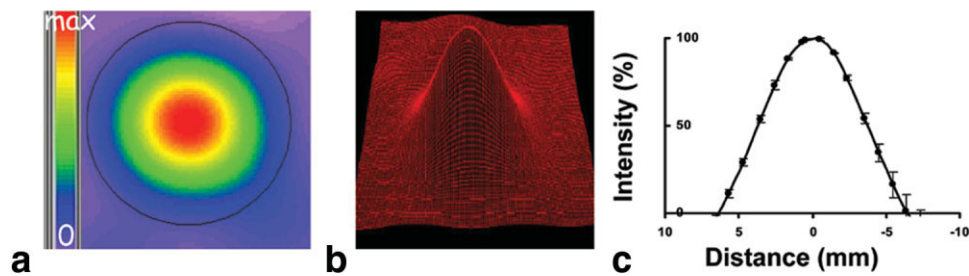
FIG. 2. EPR data obtained from a tablet of lithium formate irradiated by the insertion of one 125-iodine brachytherapy seed in the center of the tablet. **a:** 2D EPR image of the signal intensity. The color code directly reflects the gradient of dose received by this radiosensitive material. **b:** Wire-frame plot (or perspective view) of the signal intensity variation around the seed. **c:** Dose profile along the source perpendicular axis (error bars indicate mean $\pm$ standard deviation, $N = 3$).

0.8 mm wide, so it would not have made sense to compute a dose inside the source itself; and 2) the hole drilled to allow the insertion of the seed was 1.5 mm wide, so (in our model) the first meaningful dose was expected at 1 mm from the center of the phantom.

Although EPRI data generally correlated with MC simulation, several differences between these two curves can be observed.

First, the shape of the curves is different, the MC curve being narrower than the EPRI one, with a FWHM of 3.5 mm (vs. 7.2 mm for EPRI). The slope of the MC curve is very steep in the immediate vicinity of the radioactive source, becoming flatter with distance. According to the MC curve, the dose deposition at 1.7 mm is 50% and at 5.2 mm it is 90%. EPRI is a symmetric Gaussian-like curve, with 50% of dose deposition at about 3.9 mm and 90% at 5.8 mm (Fig. 4a).

Second, on the EPRI curve (Fig. 4b) it can be seen that the two maxima values are positioned at −5 mm and +5 mm (total distance between maxima is 10 mm) whereas the true location is −4 mm and +4 mm, respectively (real physical distance is 8.0 mm). This results in a shift of the two maxima points between the experimental and calculated curves.

Third, EPRI data are present even in areas where no signal would be expected, for example between −0.75 mm and + 0.75 mm (Fig. 4a); these areas correspond to the holes drilled to insert the radioactive sources, and conse-

quently they do not contain any radiosensitive material (see Discussion).

Figure 5 shows the variation of the signal in externally irradiated phantoms with a central hole of decreasing size. This allows a semiquantitative estimation of the resolution based on a visual estimation of images. Calculation of signal intensity falloff in the center of the image gives a more formal approach. For a hole of 5 mm in diameter, the signal dip on the corresponding image is 93%, the two edges of the hole being almost perfectly separated. When the size of the hole decreases, the dip decreases accordingly and falls to 46% for a 2-mm hole.

Figure 6 shows the signal intensity response along a line perpendicular to the edge of the parallelepipedic phantom used for ESF measurement (black boxes, Fig. 6b), and its derivative (black curve, Fig. 6b and c). The first half of the curve was used for the Gaussian fitting (Fig. 6d) The σ value computed for the Gaussian fit of ESF was 1.879 $\pm$ 0.019. The goodness of fit (r^2) was 0.993. The corresponding calculated FWHM was 4.4 mm.

DISCUSSION

Each radiation therapy intervention requires an accurate a priori estimation of the dose that will be delivered to the tumor and to the surrounding healthy tissues. In brachytherapy, estimation of the dose near the radioactive source is not easy. Estimation of the dose using MC calculations
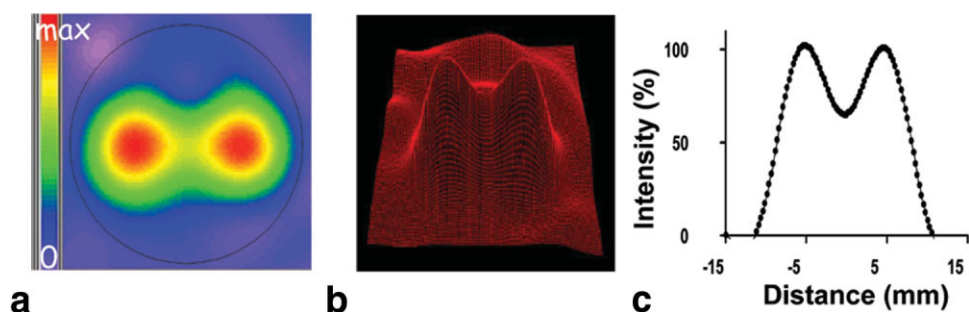
FIG. 3. EPR data obtained from a tablet of lithium formate irradiated by the insertion of two 125-iodine brachytherapy seeds. **a:** 2D EPR image of the signal intensity. The color code directly reflects the gradient of dose received by this radiosensitive material. **b:** Wire-frame plot (or perspective view) of the signal intensity variation around the seed. **c:** Distribution of dose in the plane perpendicular to the long axis of the seed, crossing the seeds in their center. The distance between the two maxima is 10 mm.
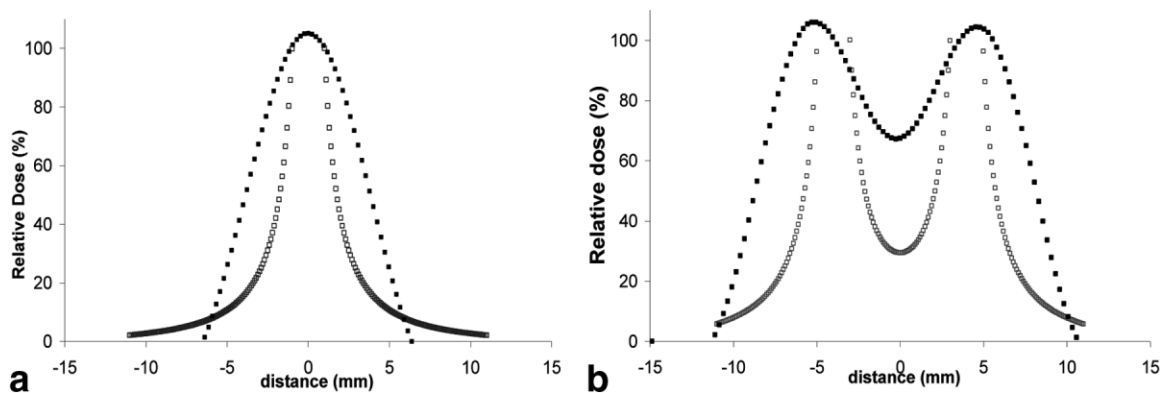
FIG. 4. **a:** Comparison of the dose distribution profiles in a tablet irradiated by one ^{125}I seed. EPRI data (black boxes) vs. Monte Carlo simulation (open boxes). **b:** Comparison of the dose distribution profiles in a tablet irradiated by two ^{125}I seeds. EPRI data (black boxes) vs. Monte Carlo simulation (open boxes).

in the close vicinity of the seeds (<1 cm) is dependent on the codes used and the underlying physics approximations. However, these estimations are particularly important for treatment planning and clinical outcome. Moreover, recent data showed that the evolution of the tumor microenvironment during brachytherapy is strongly dependent on the distance (in the first millimeters) between the irradiation seeds and the tumor tissue (27). In this work, we suggest a new experimental method based on the EPR imaging of free radicals induced by the irradiation in a solid matrix made of a radiosensitive material. Overall, the method offers linearity of response with increasing doses, high sensitivity, and reproducible homogeneity of signal in areas irradiated at the same dose.

Nevertheless, several differences are observed between EPRI experimental and MC simulated data. EPRI and MC intensity profiles have different shapes, the EPRI curve being broader than the MC curve. It is likely that the profile observed with the MC simulation is in closer agreement to the reality than the EPRI data. [125]I emits low-energy photons that are readily absorbed in tissue, and the dose

distribution pattern is expected to present a strong dose gradient. The data from the MC curve are more in agreement with this situation than those from the EPRI curve. Nevertheless, MC simulations are currently not fully validated for small distances (i.e., <5 mm).

It must also be remembered that the resolution reached with EPRI using lithium formate is definitely limited because of the rather large signal linewidth given by this particular material (~14 Gauss). Theoretically, the shortest distance (d) between two points that can be resolved in the EPR image is given by the equation

$$d = LW/G, \qquad [3]$$

where LW (mT) is the linewidth of the EPR signal and G (mT/m) is the magnitude of the gradient field. In our study, the linewidth of the signal is 1.4 mT, gradient magnitude is 300 mT/m and applying Eq. [3] gives a theoretical resolution d of $1.4/300 = 4.7 \ 10^{-3}$ m (4.7 mm). The resolution calculated in terms of the ESF is 4.4 mm, and in close agreement with the theoretical value. However, it can be intuitively observed from Fig. 5 that resolution might be better. More quantitatively, the decrease in signal intensity in the dip reaches 35% for a 1-mm hole. Based on the Rayleigh's criterion used in the field of optics, Eaton et al. (28) have proposed as a working definition that two points are resolved if there is a 17% decrease in EPR signal intensity between them.

Whatever it may be, because of this finite resolution, the experimental curve is smoothed to some extent, and globally presents a different profile. This limited resolution could also explain some other features. In the "two-seed" experiment, the distance separating the sources was 8.0 mm, whereas the distance measured on the EPR image is 10 mm. This imprecision (around 1 mm for each peak position) is most probably due to the limited resolution imposed by the signal linewidth. Another unexpected result of the EPRI data is the presence of data even for points located immediately around the seeds; for example, between −0.75 and +0.75 mm around the zero position (Fig. 4a). A hole was drilled in that position in order to place the seed, so that there was no radiosensitive material (lithium
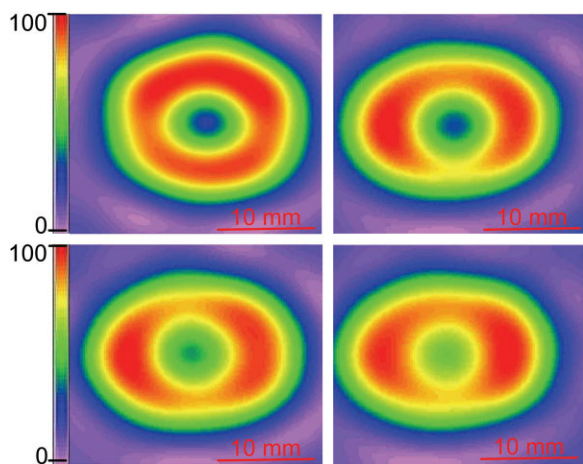
FIG. 5. 2D EPRI images of externally irradiated lithium formate phantoms. The size of the central hole is 5 mm (upper left), 4 mm (upper right), 3 mm (lower left), and 2 mm (lower right). Each image is normalized to its own maximum intensity.
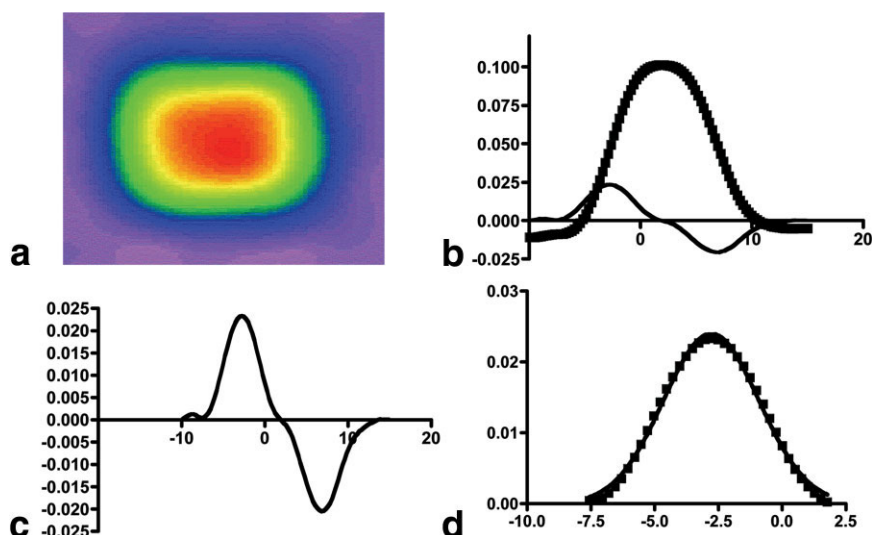
FIG. 6. **a:** 2D EPRI image using a square parallelepiped phantom. **b:** The signal response (black boxes) is obtained along a line perpendicular to the edges of the phantom. Derivative curve after smoothing (black curve). **c:** Derivative curve. **d:** First half of the derivative curve (black box) was used for Gaussian fitting (black curve).

formate) in that area. Consequently, there should not be any signal.

For this study, we used seeds containing ^{125}I. The low energy of the emitted photons is responsible for steep gradients of dose distribution. This is also the most challenging situation for EPRI since it requires accurate measurement over very small distances. Although the use of field gradients allowed evaluation of the continuous deposit of dose in the close vicinity of the seeds and the quantification of the dose gradient (Figs. 2 and 3), the resolution still requires further improvement. The accuracy of the method also has to be demonstrated.

The rationale for using lithium formate as a dosimetric material instead of alanine was based on the following considerations. First, the EPR spectrum of CO_2^- is single-lined (compared to the complex spectrum of irradiated alanine, which is not suitable for imaging purpose) (Fig.1a), making the spectrum fairly simple and particularly convenient for imaging applications. CO_2^- radicals are also reported to be extremely stable, up to 10^9 years (29,30). Second, as the lithium formate EPR spectrum is a single line, Vestad et al. (9) reported that this material gives a higher peak-to-peak signal and is six times more sensitive than alanine. This material is also tissue equivalent: the Z_{eff} are 6.78, 7.31, and 7.51 for alanine, lithium formate, and water, respectively. Moreover, it exhibits no zero-dose signal (8,9), and shows a linear dose response (Fig.1b). Finally, lithium formate can be pressed into tablets without the need for a binding agent. Other materials known to have a narrower EPR linewidth signal could be used but have several disadvantages, such as being very highly hygroscopic or not being commercially available. A high spatial resolution of 1 mm would be desirable for applicability of EPRI for clinical purpose, as radiotherapists need an accurate dosimetry in the range of 1 mm. Several different strategies could be considered. First of all, images could be acquired using a higher magnitude of the gradient field. With a gradient up to 2000 mT/m the theoretical resolution would be 0.7 mm. Enhancement of the resolution could also be achieved by using another radiosensitive material with a more narrow linewidth. On our system, the maximum field gradient is 490 mT/m. In order to reach a resolution of 1 mm, the maximum linewidth of the material should be, according to Eq. [3], 0.49 mT (490 mT/m * 0.001 m). Ammonium formate gives a ~0.65 mT (6.5 G)-width EPR signal (8), and could be investigated as a radiosensitive material for EPR imaging allowing a better theoretical resolution. Finally, it has been demonstrated that an optimized mathematical treatment of the signal before reconstruction could also greatly improve the resolution (31).

In conclusion, the present study should be considered as a first proof-of-principle that gradients of dose in the vicinity of brachytherapy seeds can be estimated using EPRI. With the present material used as a dosimetric phantom, some discrepancies were observed between MC simulations and EPRI. This is likely due to the limited resolution imposed by the signal linewidth of the material used. Better resolution would be expected with radiosensitive materials with narrower linewidths. No gold standard method is currently available to evaluate the dose distribution pattern in areas around brachytherapy sources. As there is a growing need for new methods, EPRI appears to possess interesting characteristics that demonstrate its potential in this field of investigation. The perspectives of the present study could be the development of absolute 2D and 3D quantification of doses, for example by using internal or external references. It is also likely that the present concept could be applied to evaluate the distribution of doses in other forms of radiotherapy with steep gradients in dose distribution, such as the ones that are used in intensity-modulated radiation therapy (IMRT).

ACKNOWLEDGMENTS

REFERENCES

1. Reniers B, Vynckier S, Scalliet P. Dosimetric study of the new Inter-Source 125-iodine seed. Med Phys 2001;28:2285–2288.

2. Reniers B, Verhaegen F, Vynckier S. The radial dose function of low energy brachytherapy seeds in different solid phantoms: comparison between calculations with the EGSnrc and MCNP4C Monte Carlo codes and measurements. Phys Med Biol 2004;49:1569–1582.

3. Ikeya M. New applications of electron spin resonance-dating, dosimeter and microscopy. Singapore: World Scientific; 1993.

4. Schaeken B, Scalliet P. One year of experience with alanine dosimetry in radiotherapy. Appl Radiat Isot 1996;47:1177–1182.

5. Angelis CD, Onori S, Petetti E, Piermattei A, Azario L. Alanine/EPR dosimetry in brachytherapy. Phys Med Biol 1999;44:1181–1191.

6. Schultka K, Ciesielski B, Serkies K, Sawicki T, Tarnawska Z, Jassem J. EPR/alanine dosimetry in LDR brachytherapy—a feasibility study. Radiat Prot Dosimetry 2006;120:171–175.

7. Lund A, Olsson S, Bonora M, Lund E, Gustafsson H. New materials for ESR dosimetry. Spectrochim Acta A Mol Biomol Spectrosc 2002;58:1301–1311.

8. Lund E, Gustafsson H, Danilczuk M, Sastry MD, Lund A, Vestad TA, Malinen E, Hole EO, Sagstuen E. Formates and dithionates: sensitive EPR-dosimeter materials for radiation therapy. Appl Radiat Isot 2005;62:317–324.

9. Vestad TA, Malinen E, Lund A, Hole EO, Sagstuen E. EPR dosimetric properties of formates. Appl Radiat Isot 2003;59:181–188.

10. Velan SS, Spencer RGS, Kappusamy P. Electron paramagnetic resonance oxygen mapping (EPROM): direct visualisation of oxygen concentration in tissue. Magn Reson Med 2000;43:804–809.

11. Yoshimura T, Yokoyama H, Fujii S, Takayama F, Oikawa K, Kamada H. In vivo EPR detection and imaging of endogenous nitric oxide in lipopolysaccharide-treated mice. Nat Biotechnol 1996;14:992–994.

12. Krishna MC, Devasahayam N, Cook JA, Subramanian S, Kuppusamy P, Mitchell JB. Electron paramagnetic resonance for small animals imaging applications. ILAR J 2001;42:209–218.

13. Schauer DA, Desrosiers MF, Kuppusamy P, Zweier JL. Radiation dosimetry of an accidental overexposure using EPR spectrometry and imaging of human bone. Appl Radiat Isot 1996;47:1345.

14. Storm E, Israel HI. Photon cross sections from 1 keV to 100 MeV for elements Z=1 to Z=100. In: Los Alamos Scientific Laboratory Report LA-3753. Los Alamos, NM: Los Alamos National Laboratory; 1967.

15. Hubbell J, Veigele W, Briggs E, Brown R, Cromer D, Howerton R. Atomic form factors, incoherent scattering functions, and photon scattering cross sections. J Phys Chem Ref Data 1975;4:471.

16. NCS Report 16. Monte Carlo treatment planning: an introduction. Delft, The Netherlands: Netherlands Commission on Radiation Dosimetry; 2006.

17. Briesmeister JF. A general Monte Carlo N-particle transport code, version 4C LA 13709. Los Alamos, NM: Los Alamos National Laboratory; 2000.

18. Callaghan PT. Principles of nuclear magnetic resonance microscopy. Oxford: Clarendon Press; 1991.

19. Natterer F. The mathematics of computerized tomography. New York: Wiley; 1986.

20. Everett C, Cashwell E. MCP code fluorescence-routine revision. In: Los Alamos Scientific Laboratory Report LA-5240-MS. Los Alamos, NM: Los Alamos National Laboratory; 1973.

21. Bohm T, DeLuca P, DeWerd L. Brachytherapy dosimetry of ^{125}I and [103]Pd sources using an updated cross section library for MCNP Monte Carlo transport code. Med Phys 2003;30:701–711.

22. Taylor R, Yegin G, Rogers D. Benchmarking BrachyDose: Voxel based EGSnrc Monte Carlo calculations of TG-43 dosimetry parameters. Med Phys 2007;34:445–457.

23. McRobbie D, Moore E, Graves M, Prince M. MRI: from picture to proton. Cambridge: Cambridge University Press; 2003. 380 p.

24. Ahn K-H, Halpern HJ. Simulation of 4D spectral-spatial EPR images. J Magn Reson 2007;187:1–9.

25. Ahn K-H, Halpern HJ. Object dependent sweep width reduction with spectral-spatial EPR imaging. J Magn Reson 2007;186:105–111.

26. Ahn K-H, Halpern HJ. Spatially uniform sampling in 4-D EPR spectral-spatial imaging. J Magn Reson 2007;185:152–158.

27. Cron GO, Beghein N, Crokart N, Chavée E, Bernard S, Vynckier S, Scalliet P, Gallez B. Changes in the tumor microenvironment during low-dose-rate permanent seed implantation iodine-125 brachytherapy. Int J Radiat Oncol Biol Phys 2005;63:1245–1251.

28. Eaton G, Eaton S, Ohno H. EPR imaging and in vivo EPR. Boca Raton, FL: CRC Press; 1991. 336 p.

29. Schwarcz HP. ESR studies of tooth enamel. Nucl Tracks Radiat Meas 1985;10:865–867.

30. Skinner AR, Blackwell BAB, Chasteen ND, Shao J, Min SS. Improvements in dating tooth enamel by ESR. Appl Radiat Isot 2000;52:1337–1344.

31. Hirata H, Wakana M, Susaki H. Feasibility study of superresolution continuous-wave electron paramagnetic resonance imaging. Appl Phys Lett 2006;88:254103.